April, 1986

LIDS-P-1547

MULTI-VARIABLE CONTROL OF THE GE T700 ENGINE USING THE LQG/LTR DESIGN METHODOLOGY[1]

William H. Pfeil[2], Michael Athans[3], H. Austin Spang, III[4]

In this paper we examine the design of scalar and multi-variable feedback control systems for the GE T700 turboshaft engine coupled to a helicopter rotor system. A series of linearized models are presented and analyzed. Robustness and performance specifications are posed in the frequency domain. The LQG/LTR methodology is used to obtain a sequence of three feedback designs. Even in the single-input single-output case, comparison of the current control system with that derived from the LQG/LTR approach shows significant performance improvement. The multi-variable designs, evaluated using linear and nonlinear simulations, show even more potential for performance improvement.

1. INTRODUCTION

In this paper we summarize, [1], three distinct feasibility studies related to the design of feedback control systems for a model of the GE T700 turboshaft engine coupled to a helicopter rotor system. The present control system on the T700 engine uses a single input, the fuel, and was designed using classical single-input single-output (SISO) techniques. We explore the potential advantages of using more sophisticated compensators, derived using the Linear-Quadratic-Gaussian with Loop-Transfer-Recovery (LQG/LTR) design methodology, both in the SISO case and in the multiple-input multiple-output (MIMO) case. In the MIMO case we use the dynamic coordination of both fuel and variable compressor geometry to control two outputs of interest.

To the best of our knowledge this is the first study dealing with the application of multi-variable design concepts to a turboshaft engine. On the other hand, the modern multivariable control of turbofan engines has received a great deal of attention. The book by Sain et al, [2], contains a variety of design studies on the F-100 turbofan engine; other pertinent references are [3] to [11]. In particular, feasibility studies using the LQG/LTR design methodology have been reported for the F-100 engine in [3] and [4], the GE-21 engine in [5], and the GE-16 engine in [6]. There seems to exist widespread agreement that the dynamic coordination of fuel with several engine geometry variables will result in future multi-variable feedback designs that will improve engine efficiency, result in more rapid thrust response, tighter control of key temperatures and pressures, and improved stall margins.

The dynamic models used in this study include the interaction between the turboshaft engine and the helicopter main-rotor and tail-rotor dynamics. As explained in Section 2, we included the engine-rotor dynamic interactions in our model because the bandwidth specifications, that we have imposed to carry out our feasibility studies, were larger than those of the production design, and consequently the resonances associated with the main and tail rotor dynamics had to be included in our model. On the other hand, precise knowledge of such resonances is not available. For this reason, we have estimated engine-rotor model errors in the frequency domain, and imposed stability-robustness specifications, so as to account for such modeling errors. We do not claim that we have captured all relevant high frequency modeling errors; nonetheless, a similar stability-robustness analysis will have to be carried out in a more realistic application.

We present evaluations of three distinct feasibility studies for the engine-rotor system. Design A is a SISO design using the LQG/LTR method. In Design A we use only the fuel to control the free (power) turbine speed. We compare the "sophisticated" Design A with the existing production design, and demonstrate improved performance. Thus, there exists potential performance payoff in using, even in

1. This research was performed at the MIT Laboratory for Information and Decision Systems with support provided by the General Electric Company and by the NASA Ames and Langley Research Centers under grant NASA NAG2-297.

2. Mail Stop 34041, General Electric Co., Aircraft Engine Business Group, 1000 Western Ave., Lynn, MA, 01910

3. Department of EE&CS, Room 35-406, MIT, Cambridge, MA 02139

4. Corporate Research and Development Center, General Electric Co., Schenectady, NY 12345; also, Adjunct Professor, Dept. of EE&CS, MIT.

Proceeding American Control Conference, Seattle, WA, June 1986.

a SISO setting, dynamic models of greater fidelity and more sophisticated compensator designs.

Design B is a MIMO design, and it is used to demonstrate the advantages of using an additional control variable. We use the dynamic coordination of both fuel and variable compressor geometry to independently control the free turbine speed and the gas generator speed. We compare the MIMO Design B to the SISO Design A with respect to their disturbance rejection properties. We show that Design B is superior in the sense that dynamic modulation of the variable geometry control is utilized to reject disturbances. The same disturbance in the SISO design would have to modulate the fuel, thereby possibly decreasing the engine fuel efficiency.

Design C is a different MIMO design. Like Design B we again use both the fuel and variable geometry as dynamic controls. However, in Design C the outputs that we wish to control are the free turbine speed and the inter-turbine gas temperature. Precise control of temperature is necessary when the engine operates at high-power conditions so as to prevent damage. With this choice of controls and outputs the engine-rotor open-loop dynamics exhibit a non-minimum phase zero at about 0.2 rad/sec. The presence of this non-minimum phase zero imposes limitations with respect to the command-following and disturbance-rejection performance of the feedback system. Nonetheless, we demonstrate that slow temperature trim commands, useful for dynamically improving engine efficiency, can be reasonably followed.

At this point it is important to stress that the results presented in this paper only represent feasibility studies, and more work is needed before the LQG/LTR based compensators are implemented in a working control system. Although we have used non-linear simulations to evaluate the designs, we did not test them over the full envelope of possible operating conditions. It is likely that gain-scheduling will have to be used to develop designs that maintain improved performance and stability over the full operating envelope. In spite of these limitations, the results demonstrate significant advantages of using multi-variable control for turboshaft engine applications, and illustrate the types of compensators that would result from the LQG/LTR design methodology [12] to [17].

The remainder of the paper is organized as follows. In Section 2 we present a discussion of the GE T700 turboshaft engine dynamics and its dynamic coupling to the helicopter rotor system, including a discussion of the nature of the linearized dynamics. In Section 3 we present an analysis of the linearized dynamics for the three designs, in terms of poles and zeros, and frequency domain singular value plots. In Section 3 we also quantify the modeling errors in the rotor dynamics so that we can impose stability-robustness specifications in the frequency domain; in addition, we summarize the idealized performance specifications that we imposed for our feasibility studies. In Section 4 we first present a brief overview of the LQG/LTR design methodology which was used for deriving the Designs A, B, and C. In Section 5 we summarize the characteristics of all three designs in the frequency domain by presenting the shapes of the singular values of the loop, sensitivity, and closed-loop transfer function matrices vs. frequency. Then, we evaluate the transient performance characteristics via simulation. Section 6 summarizes the conclusions. The appendix contains the state equations and the numerical values of the open-loop dynamics in terms of the A, B, C, D matrices of the state-space models.

2. SYSTEM DESCRIPTION AND MODEL FORMULATION

2.1 System Description

A conventional helicopter, as shown in Figure 1, utilizes a single main rotor, primarily for lift, and a tail rotor for torque reaction and directional control in the yaw degree of freedom. The main and tail rotor systems are directly coupled to two turboshaft engines through gear reduction sets and shafting.

The main and tail rotor systems are composed of individual blades which are simply airfoils that provide lift and/or thrust. The pilot maneuvers the helicopter by modulating the available lift/thrust from the rotor systems. A maneuvering demand from the pilot is equivalent to producing a load disturbance on the rotor systems. Load disturbances may also emanate from other sources such as wind gusts. The incorporation of a "fast" or "tight" engine speed control capable of rejecting rotor system load disturbances will be reflected in increased helicopter maneuvering capability. This increased maneuvering capability must be accomplished, however, without exciting coupled engine/rotor system complaint dynamics that are present.

The turboshaft engine utilized in this study is the GE T700 engine, as representative of a recent technology engine in current production. A simplified cross-section of the GE T700 is shown in Figure 2. The gas generator sustains the gas turbine cycle, while the free turbine performs the role of extracting energy. It is the free turbine, when directly coupled to the helicopter rotor system, that recovers the useful work of the gas turbine cycle. The responsibility of the gas generator is to provide the power demanded by the helicopter rotor systems at a specified free turbine speed. The turboshaft engine control system must insure that the power demanded by the helicopter rotor system is

supplied by the engine while simultaneously insuring that the engine operates efficiently over a wide range of ambient conditions and prevents destructive stall phenomenon, turbine overtemperatures, overspeeds and excessive shaft torque. On the GE T700 two control variables, fuel flow and compressor variable geometry, can be utilized to meet these objectives. In the current control system only the fuel is controlled in a closed-loop sense. The compressor variable geometry is scheduled in an open-loop manner.

The operational requirements for the turboshaft engine are summarized below:

The engine must:

1. Maintain constant free turbine speed in the presence of load disturbances to the helicopter rotor systems,
2. Not provide input energy to excite coupled engine/drive train resonant modes,
3. Maintain adequate stall margin,
4. Limit turbine inlet temperatures, speed and torque, and
5. Operate at peak efficiency.

The remainder of this paper overviews the results of research [1] undertaken to examine the feasibility of the LQG/LTR control design methodology in achieving the above goals.

2.2 Model Formulation

Turbine engine dynamics are described by complex non-linear equations relating state variables $\underline{x}(t)$, control variables $\underline{u}(t)$, output variables $\underline{y}(t)$ and ambient variables in the form

$$d/dt\, \underline{x}(t) = \underline{f}(\underline{x}(t), \underline{u}(t), \underline{\theta}) \qquad (1a)$$

$$\underline{y}(t) = \underline{g}(\underline{x}(t), \underline{u}(t), \underline{\theta}) \qquad (1b)$$

The state variables are associated with energy storage elements and are temperatures, pressures and inertia terms for a gas turbine system. The control inputs are fuel flow and variable geometries. The outputs can be turbine speeds, pressure ratios and gas temperatures. The ambient variables are ambient pressure and temperature ratios.

Prior to formulation of the control problem, the non-linear dynamic description must be converted to a linear dynamic model pertinent to operation about an equilibrium operating condition. The equilibrium condition is characterized by $\underline{\theta}$ and the steady-state values of the state, control and output variables ($\underline{x}_o$, $\underline{u}_o$, $\underline{y}_o$).

The linear, time-invariant, constant coefficient model utilized in the subject research is of the form

$$d/dt\, \delta \underline{x}(t) = \underline{A}\, \delta\, \underline{x}(t) + \underline{B}\, \delta\, \underline{u}(t) \qquad (2a)$$

$$\delta \underline{y}(t) = \underline{C}\, \delta\, \underline{x}(t) + \underline{D}\, \delta\, \underline{u}(t) \qquad (2b)$$

where

$$\underline{A} = \left.\frac{\partial \underline{f}}{\partial \underline{x}}\right|_{\substack{\underline{x}_o \\ \underline{u}_o}} ; \quad \underline{B} = \left.\frac{\partial \underline{f}}{\partial \underline{u}}\right|_{\substack{\underline{x}_o \\ \underline{u}_o}}$$

$$\underline{C} = \left.\frac{\partial \underline{g}}{\partial \underline{x}}\right|_{\underline{x}_o} ; \quad \underline{D} = \left.\frac{\partial \underline{g}}{\partial \underline{u}}\right|_{\underline{x}_o}$$

The objective in model formulation is to establish a nominal representation of the open-loop system, or plant, in the low frequency region where performance specifications are imposed. To achieve a practical and implementable design, the coupled engine/helicopter dynamics in the 0-40 rad/sec frequency range were examined for inclusion in the nominal linear model. The two available control variables, fuel flow, W_f, and compressor variable geometry, V_g, were included in the model representation to provide independent control of two output variables (to be discussed later).

The low frequency (< 10 rad/sec) GE T700 engine dynamics are dominated by the gas generator and free turbine dynamics. Pressure and temperature dynamics appearing in the flow equations are typically "fast" for a small turboshaft engine and are included in the model only as outputs, thus neglecting their dynamics. Inter-turbine gas temperature, $T_{4.5}$, was included in the model as an output as it is often desired to control that variable. The reduced engine state vector for design purposes is thus given simply by the two turbine speeds: the gas generator speed, N_g, and the free turbine speed, N_p.

The helicopter drive train compliant dynamics must be represented in the system model because they are present within the engine response bandpass. A representative helicopter drive train is shown isometrically in Figure 3. A simplified, lumped parameter, spring-mass-damper representation of the system is shown in Figure 4.

The turboshaft engines are coupled to the helicopter drive-train model as shown in Figure 5, which is a block diagram representation of the coupled system. Note that the only coupling is through Q_p, which is the gas torque generated by the gas generator and applied at the power turbines. The state variable representation of Figure 5 is given in Appendix A. The variable def-

initions for Figure 5 with units are included in Table 1. The full model also includes $T_{4.5}$ sensor and V_g actuator dynamics.

A series of linear models were generated representing a range of operating conditions. The operating conditions are defined by power level or percent of design gas generator speed.

3. SYSTEM DEFINITIONS, ROBUSTNESS REQUIREMENTS, AND DESIGN SPECIFICATIONS

3.1 System Definitions

Three distinct open-loop system definitions are presented for utilization in controller design. The first (System A) is a conventional SISO system with scalar fuel flow control (W_f) and a single scalar output, the free turbine speed, N_p. With two available control inputs, fuel flow, W_f, and variable geometry position, V_g, control over two distinct output variables is realizeable. Accordingly, the second system definition (System B) explores the simultaneous control of free turbine, speed, N_p and gas generator speed, N_g. The third system definition (System C) represents an exploration into the simultaneous control of free turbine speed and inter-turbine gas temperature, $T_{4.5}$.

The control of power turbine speed is required to satisfy the fundamental system requirement of a commanded power supply to the helicopter rotor systems. In System B, the simultaneous control of the power turbine and gas generator speeds was undertaken to explore the utilization of this control system definition for both input and output disturbance rejection as compared to the SISO controller. The simultaneous control of turbine temperature in System C allows a potential handle on dynamic engine operational efficiency and provides some latitude in temperature limiting.

The input-output definitions are summarized in Table 2 along with the operating conditions for the linear dynamic model utilized for each design as denoted by the power level or % N_g. The 90% N_g design model was chosen for the SISO design (System A) because it is representative of normal operating power. The 83% N_g design model level was utilized for MIMO System B to examine the implications of a MIMO control law at a low power level. The 90% N_g design model was chosen for MIMO System C because it is, as mentioned previously, representative of normal operating power. The linearized equations for each system are summarized in Appendix B.

The poles and zeros of the design models for each system definition are tabulated in Table 2. The zeros for the multi-variable system definition are transmission zeros [13]. Note that System C has a non-minimum phase zero at .199 rad/sec which presents a generic performance limitation [20] that will become clearly evident in the controller design results section.

Figures 6 to 8 display the singular values of the three open-loop Systems A, B, and C respectively. Thus, we plot the singular values [17]

$$\sigma_i [\underline{G}_p (j\omega)] \tag{3}$$

where

$$\underline{G}_p (s) = \underline{C} (s \underline{I} - \underline{A})^{-1} \underline{B} + \underline{D} \tag{4a}$$

$$\underline{y} (s) = \underline{G}_p (s) \underline{u} (s) \tag{4b}$$

is obtained from the linear models in Appendix B. All three frequency plots show the effects of main rotor and tail rotor resonances. Also note that (see Figure 8) the presence of the non-minimum phase zero for System C manifests itself in a small minimum singular value at low frequencies, as compared to Systems A and B.

3.2 Robustness Requirements

The dominant high-frequency uncertainty in the linear model is in the description of the helicopter rotor dynamics. The rotor system lumped parameter model does not portray the functional relationships of the main rotor spring and damping coefficients with helicopter flight condition, rotor coning angle, etc. The posing of a maximum realizeable range of coefficient variation, while not capturing the explicit functional relationships, will acknowledge their presence and provide the basis for a conservative, stable design.

Consider the actual plant, $\tilde{\underline{G}} (s)$ to be related to the linear model representation, by the expression

$$\tilde{\underline{G}} (s) = \underline{L} (s) \underline{G}_p (s) \tag{5}$$

Equation (5) relates the model uncertainty quantified by $\underline{L} (s)$ to the system output variables as shown in Figure 9.

For the error defined by Equation (5), an output feedback system is guaranteed to be stable if the inequality

$$\sigma_{max} [\underline{L}(j\omega) - \underline{I}] \leq \sigma_{min} [\underline{I} + (\underline{G}_p(j\omega) \underline{K}(j\omega))^{-1}] \tag{6}$$

is satisfied for all ω [18, 19], where $\underline{K}(j\omega)$ is the compensator transfer function matrix. The error matrix, $\underline{L}(j\omega)$, will be assumed to be of the form

$$\underline{L}(j\omega) = \underline{I} + \underline{E}(j\omega) = \underline{I} + \text{diag} [e_r(\omega), e_e(\omega)] \tag{7}$$

where

$e_r(\omega)$ = rotor system error

$e_e(\omega)$ = engine system error.

The above error structure reflects the uncertainty of the high frequency rotor system description to the power turbine speed output. The error in the low frequency engine system will be assumed small and we will let $e_e(\omega) = 0$.

The construction of $e_r(\omega)$ to quantify rotor system parametric variations is best visualized on a polar plot (Nyquist Diagram) of the rotor system open-loop transfer function as shown in Figure 10. The rotor system dynamics are present in the system transfer function matrix for free turbine speed output and for both control variables W_f and V_g. Realizeable rotor system variations perturb the nominal system representation. A circle of radius r and center coincident with the nominal model encompassing the family of perturbed plants at several frequencies is also shown in Figure 10. The function relationship of the magnitude of r with frequency establishes $e_r(\omega)$. The function $e_r(\omega)$ thus quantifies the realizable magnitude variations of the rotor system representation so that a compensated system can be designed that does not realize a change in the number of encirclements of the critical point on the Nyquist Plot. A change in the number of encirclements is indicative of instability, and will be avoided if the inequality presented by Equation (6) is satisfied. A logarithmic plot of $e_r(\omega)$ is shown explicitly in Figure 11.

3.3 Design Specifications

The implication of specifications is to achieve good performance in terms of

1. command following,
2. disturbance rejection, and
3. insensitivity to modeling error through the introduction of feedback.

For a feedback system, as shown in Figure 12, the maximum error at a given frequency, ω_0, for unit magnitude commands and output disturbances is given by

$$\| \underline{e} \|_2 = 1/\sigma_{min}[\underline{I} + \underline{T}(j\omega_0)] \qquad (8)$$

where

$$\underline{T}(j\omega_0) = \underline{G}(j\omega_0)\,\underline{K}(j\omega_0).$$

If $\sigma_{min}\,\underline{T}(j\omega_0) \gg 1$, then Equation (8) is nearly

$$\| \underline{e} \|_2 = 1/\sigma_{min}\,\underline{T}(j\omega_0). \qquad (9)$$

Intuitively, by making $\sigma_{min}\,\underline{T}(j\omega_0)$ "large" over a wide frequency range, we can both reject output disturbances and follow commands with small errors. This performance consideration must be tempered with a bandwidth limitation. (i.e. when $\sigma_{min}\,\underline{T}(j\omega_0) = 1$) so that unmodeled dynamics do not cause instability. A desirable crossover frequency for this system, as derived from pilot evaluations [21] is about 10 rad/sec. To provide maximum command following and disturbance rejection, it is desired that

$$\sigma_{min}\,\underline{T}(j\omega) > 20\text{db}\ \forall\ \omega \leq 1\ \text{rad/sec}. \qquad (10)$$

It is also required that all output variables have zero steady-state error to constant reference inputs, thus dictating integral augmentation.

Figure 13 summarizes the frequency domain performance specifications. Robustness will be achieved through satisfaction of the inequality presented in Equation (6).

The above specification should be viewed as tentative. It is well recognized by now that the presence of low-frequency non-minimum phase zeros (as we have for System C) represents a generic limitation in performance independent of the design methodology employed. As we shall see in the next section, we will not be able to meet the specification above for System C.

The following sections present the design methodology and the controllers designed to meet the specifications.

4. LQG/LTR DESIGN METHODOLOGY OVERVIEW

The control structure to be utilized, including integral augmentation, is shown in Figure 14. The LQG/LTR compensation to be designed is given by $\underline{K}_D(s)$. The overall compensator, which includes integral augmentation, is defined by

$$\underline{K}(s) = (\underline{I}/s)\,\underline{K}_D(s). \qquad (11)$$

For design purposes, the integral augmentation is considered part of the plant, thus we define:

$$\underline{G}_a(s) = \underline{G}_p(s)\,(\underline{I}/s). \qquad (12)$$

The LQG/LTR procedure begins with the state description of the augmented plant given by

$$d/dt\,\underline{x}_a(t) = \underline{A}_a\,\underline{x}_a(t) + \underline{B}_a\,\underline{u}_a(t) \qquad (13a)$$

$$\underline{y}_a(t) = \underline{C}_a\,\underline{x}_a(t) \qquad (13b)$$

and thus

$$\underline{G}_a(s) = \underline{C}_a\,(s\underline{I} - \underline{A}_a)^{-1}\,\underline{B}_a. \qquad (13c)$$

The step-by-step LQG/LTR [16, 17] design procedure to define the compensator $\underline{K}_D(j\omega)$ is:

Step 1: Shape the Kalman Filter Loop Transfer Function $\underline{G}_{KF}(j\omega)$ given by

$$\underline{G}_{KF}(j\omega) = \underline{C}_a (j\omega \underline{I} - \underline{A}_a)^{-1} \underline{H}_a \qquad (14)$$

where $\underline{H}_a$ = Kalman Filter Gain Matrix using the free parameters $\underline{L}$ and μ available in the Kalman Filter algebraic Riccatti equation

$$\underline{A}_a \underline{\Sigma} + \underline{\Sigma} \underline{A}_a + \underline{L} \underline{L}^T - (1/\mu) \underline{\Sigma} \underline{C}_a^T \underline{C}_a \underline{\Sigma} = \underline{0} \quad (15)$$

to yield the gain matrix

$$\underline{H}_a = (1/\mu) \underline{\Sigma} \underline{C}_a \qquad (16)$$

so that the performance specifications posed in Section 3 are met.

Step 2: Solve the following algebraic Riccatti equation.

$$\underline{K} \underline{A}_a + \underline{A}_a^T \underline{K} + q \underline{C}_a^T \underline{C}_a - \underline{K} \underline{B}_a \underline{B}_a^T \underline{K} = \underline{0} \quad (17)$$

for $q \rightarrow \infty$ (sufficiently large) to yield the control gain matrix

$$\underline{G}_a = \underline{B}_a^T \underline{K}. \qquad (18)$$

As $q \rightarrow \infty$ the LQG/LTR method guarantees that in the absence of non-minimum phase zeros

$$\underline{T}_a(s) = \underline{G}_a(s) \underline{K}_D(s) \approx \underline{G}_{KF}(s). \qquad (19)$$

Thus if we design $\underline{G}_{KF}(j\omega)$ to meet the posed frequency domain performance specifications, and there are no non-minimum phase zeros in the system, then we can design a compensator, defined by

$$\underline{K}_D(s) = \underline{G}_a (s \underline{I} - \underline{A}_a + \underline{B}_a \underline{G}_a + \underline{H}_a \underline{C}_a)^{-1} \underline{H}_a \quad (20)$$

by utilizing the asymtotic adjustment procedure (i.e. "cheap" LQG control problem) defined in Step 2. The presence of a non-minimum phase zero within the desired bandwidth of the system presents a generic performance limitation that cannot be considered an indictment of this methodology. The restrictions presented by a non-minimum phase zero within the desired system bandwidth will be demonstrated in the following section.

5. CONTROLLER DESIGN RESULTS

5.1 SISO Design A

For the SISO system definition with scalar fuel flow control over the free turbine speed, the application of a generalization of the design methodology presented in Section 4 to the SISO case results in the loop transfer function shown in Figure 15. The system is shown to achieve the desired performance specifications. The compensator transfer function is shown in Figure 16. It is readily seen by comparison of the open-loop SISO transfer function of the plant shown in Figure 6 with the compensator transfer function of Figure 16, that the LQG/LTR design methodology performs an approximate inversion of the open-loop plant [17]. Robustness is achieved as shown in Figure 17 for the modeling errors quantified in Section 3.

A comparison using nonlinear dynamics was performed to determine the increase in system performance achievable with a LQG/LTR controller vs. a lower bandwidth, conventional controller. Figure 18 displays a typical helicopter transient, a 30% load demand performed in 1 sec., for both a LQG/LTR and the current conventional controller. The fact that the LQG/LTR controller provides "tighter" power turbine speed governing is readily observed by comparing the power turbine speed deviations shown in Figures 18a and 18b. The improvement can be quantified by noting that the sensitivity transfer function, given by

$$1/(1 + g(s)\, k(s)) \qquad (21)$$

and shown in Figure 18c, which is indicative of the systems response to load disturbances, provides load disturbance attenuation over a much wider range of frequencies than does the conventional controller.

5.2 MIMO System B Design

The first MIMO design, providing the coordinated control of the power turbine and gas generator speeds using the fuel flow and variable geometry inputs, is presented to demonstrate not only the LQG/LTR design methodology, but to demonstrate how the coordinated control of several variables can provide a performance not realizeable with conventional scalar controls.

The loop transfer function designed for this system definition is shown in Figure 19. Note that the performance specifications are met. Robustness, for the modeling errors quantified in Section 3, is achieved as shown in Figure 20. The MIMO compensator transfer function $\underline{K}_D(j\omega)$ is shown in Figure 21. Note, as in the SISO case, that the compensator, $\underline{K}_D(j\omega)$, is an approximate inversion of the open-loop plant shown in Figure 7. The closed-loop and sensitivity singular value plots are shown in Figure 22 and 23, respectively. The closed-loop and sensitivity singular value plots demonstrate that good command following and disturbance rejection is realized.

It is instructive to perform a comparison between this MIMO system definition and the SISO system

definition in terms of the ability of these systems to reject disturbances. The basis for comparison will be to determine if it is possible, by using the coordinated control of several variables, to provide a system that exhibits disturbance rejection capability without the extensive use of control energy. If we consider that the variable geometry input variable is available at no cost to the user, then any use of the variable geometry input can be considered a savings of fuel.

It is possible to incur a disturbance in the gas generator speed due to power extraction or engine inlet distortion. A linear simulation of the response of MIMO Design B to a step disturbance on gas generator speed is shown in Figure 24a. A linear simulation of the same disturbance to the SISO design A is shown in Figure 24b. Note that while both the MIMO and SISO systems reject the gas generator speed disturbance, the MIMO system rejects the disturbance rapidly and with no steady-state fuel cost as is incurred in the SISO system.

The comparison between the MIMO and SISO case is instructive in pointing out that extended system performance capabilities are possible through the coordinated control of several variables, provided that no generic limitations induced by non-minimum phase zeros exist.

5.3 MIMO System C Design

MIMO System C provides for the control of both the power turbine and inter-turbine gas temperature, using the fuel flow and variable geometry controls. A non-minimum phase zero is present at .199 rad/sec in this design model due to the interaction of the variable geometry and airflow/temperature dynamics in the engine. The singular value loop transfer function for this design is shown in Figure 25. Note that the posed performance specifications cannot be met. This is due to the presence of the non-minimum phase zero at .199 rad/sec which limits the frequency range for which $\sigma_{min}\, \underline{T}(j\omega)$ can be made "large". The system is robust however, for the modeling errors defined in Section 3 as shown in Figure 26. The closed-loop and sensitivity plots are shown in Figures 27 and 28, respectively. Note that the effect of the non-minimum phase zero is demonstrated in all singular value plots.

A trim signal on the inter-turbine gas temperature reference, a 10-second ramp of 20°F, as performed on a non-linear simulation is shown in Figure 29. The error magnitude between the temperature reference and the sensed temperature is determined by $\sigma_{min}\, \underline{T}(j\omega)$ as presented by Equation (9). The 10-second ramp trim signal was chosen to represent the fact that the command error magnitude could be maintained at a relatively small level if the trim command signal is in the frequency range for which $\sigma_{min}\, \underline{T}(j\omega)$ is "large".

5.4 Design Summary

Three important issues were demonstrated in this section. The first is that the LQG/LTR design methodology provided a systematic approach to frequency domain 'loop shaping' for both the SISO and MIMO case. Additionally it was shown that the coordinated control of several variables can be utilized to provide performance not achievable with conventional scalar controls. Finally, the generic performance limitations of non-minimum phase zeros were demonstrated.

6. CONCLUSIONS

In this paper we have examined both SISO and MIMO designs for the control of a model of the GE T700 turboshaft engine including its dynamic coupling to the rotors of a helicopter. All control system designs were carried out using the so-called LQG/LTR design methodology. The results indicate that there is potential for significant payoff in command-following and disturbance-rejection performance, if realistic models of the engine-rotor system are used in the design process. It was also demonstrated that the dynamic coordination of both fuel and variable geometry controls results in superior performance. There was no particular difficulty in applying the LQG/LTR procedure to these designs, even when the plant had non-minimum phase zeros (Design C). In the latter case, the results were predictable and consistent with the limitations in performance inherent in non-minimum phase systems.

We reiterate that our results should be viewed as feasibility studies. Much more work is needed to design a full envelope control system for the engine-rotor dynamic system.

7. ACKNOWLEDGMENT

The authors are grateful to Dr. Gunter Stein for his numerous discussions and suggestions.

REFERENCES

(1) Pfeil, W., "Multivariable Control for the GE T700 Engine Using the LQG/LTR Methodology", S.M. Thesis, Massachusetts Institute of Technology, Cambridge, June 1984.

(2) Sain, M.K., et al (eds), "Alternative for Linear Multivariable Control", National Engineering Consortium, Chicago, 1978.

(3) Kappos, E., "Robust Multivariable Control for the F-100 Engine", S.M. Thesis (LIDS-TH-1328), Massachusetts Institute of Technology, Cambridge, Sept. 1983.

(4) Athans, M., et al, "Linear-Quadratic Gaussian with Loop Transfer Recovery Methodology for the F-100 Engine", I.E.E.E. Journal of Guidance and Control, Vol. #9, No. 1, Jan.-Feb. 1986, pp. 45-52.

(5) Kapasouris, P., "Gain-Scheduled Multivariable Control for the GE-21 Turbofan Engine Using the LQR and LQG/LTR Methodologies", S.M. Thesis (LIDS-TH-1380), Massachusetts Institute of Technology, Cambridge, May 1984.

(6) Dunn, F., "Multivariable Design of Advanced Jet Engines Using the LQG/LTR Design Methodology", S.M. Thesis, Massachusetts Institute of Technology, Cambridge, June 1986.

(7) DeHoff, R.L., et al, "F-100 Multivariable Control Synthesis Program", Vol. I, AFAPL TR-77-35, 1976.

(8) Miller, R.J. and Hackney, R.D., "F-100 Multivariable Control System Engine Models/Design Criteria", AFAPL TR-76-74, 1976.

(9) Szuch et al, "F-100 Multivariable Control Synthesis Program-Evaluation of a Multivariable Control Using a Real-Time Engine Simulation", NASA TP 1056, 1977.

(10) Idelchik, M., "An Application of Modern Control Theory to a High-Bypass Variable Compressor Geometry Engine", S.M. Thesis (LIDS-TH-1127), Massachusetts Institute of Technology, Cambridge, July 1981.

(11) Brown, H. and Fisk, W., "Integrated Flight and Propulsion Operating Modes for Advanced Fighter Engines", ASME P83-GT-194.

(12) Athans, M., "The Role and Use of the LQG Problem in Control System Design", IEEE Transactions on Auto. Control, Vol. AC-16, Dec. 1971, pp. 529-552.

(13) Kwakernaak, H., and Sivan, R., "Linear Optimal Control Systems", John Wiley & Sons, New York, 1972.

(14) Doyle, J.C. and Stein G., "Multivariable Feedback Design: Concepts for a Classical Modern Synthesis", IEEE Transactions on Auto. Control, Vol. AC-26, Feb. 1981, pp. 4-16.

(15) Stein, G., "LQG-Based Multivariable Design Frequency Domain Interpretation", AGARD-LS-117 NATO, 1981.

(16) Stein G. and Athans, M., "The LQG-LTR Procedure for Multivariable Feedback Control Design", Rept. LIDS-R-1384, Massachusetts Institute of Technology, Cambridge.

(17) Athans, M., "Lecture Notes on Multivariable Control Systems: MIT Subject 6.232", Massachusetts Institute of Technology, Cambridge, 1984.

(18) Lehtomaki, N.A., "Practical Robustness Measures in Multivariable Control System Analysis", Ph.D. Thesis (LIDS-TH-1093), Massachusetts Institute of Technology, Cambridge, May 1981.

(19) Lehtomaki, N.A., Sandel Jr., N.R., and Athans, M., "Robustness Results in LQG-Based Multivariable Control Design", IEEE Transactions on Automatic Control, Vol. AC-26, Feb. 1981, pp. 75-92.

(20) Freudenberg, J.S. and Looze, D.P., "Right Half Plane Poles and Zeros and Design Tradeoffs in Feedback Systems", IEEE Transactions on Auto. Control, Vol. AC-30, June 1985.

(21) Corliss, L.D., "A Helicopter Handling Qualities Study of the Effects of Engine Response Characteristics, Height Control Dynamics, and Excess Power on Nap-of-the-Earth Operations", presented at the AHS/NASA Specialists Meeting on Helicopter Handling Qualitities, Palo Alto, CA, 1982.Transactions on Auto. Control, Vol. AC-16, Dec. 1971, pp. 529-552

TABLE 1. *VARIABLE DEFINITIONS*

D_{AM}	= Main Rotor Aerodynamic Damping, ft.-lbs/RPM
D_{AT}	= Tail Rotor Aerodynamic Damping, ft.-lbs/RPM
D_{MR}	= Main Rotor Damping, ft.-lbs./RPM
J_{MR}	= Main Rotor Inertia, ft.-lb.-sec./RPM
J_T	= Lumped Drive Train Inertia, ft.-lb.-sec./RPM
J_g	= Gas Generator Inertia, ft.-lb.-sec/RPM
K_{MR}	= Main Rotor Spring Constant, ft.-lbs./RPM-sec
K_{TR}	= Tail Rotor Spring Constant, ft.-lbs./RPM-sec
N_{MR}	= Main Rotor Speed, RPM
N_{TP}	= Tail Rotor Speed, RPM
N_g	= Gas Generator Speed, RPM
N_p	= Free Turbine Speed, RPM
Q_{MR}	= Main Rotor Torque, ft.-lbs.
Q_{TR}	= Tail Rotor Torque, ft.-lbs.
Q_g	= Gas Generator Gas Torque, ft.-lbs.
Q_p	= Power Turbine Gas Torque, ft.-lbs.
$T_{4.5}$	= Interturbine Gas Temperature, degrees R
T_{TC}	= Thermocouple Lag, 1/sec.
T_{VG}	= Variable Geometry Actuator Lag, 1/sec.
V_g	= Variable Geometry Position, degrees
V_{ge}	= Variable Geometry Input Command, degrees
W_f	= Fuel Flow, lb./hr.

TABLE 2. *OPEN-LOOP POLE-ZERO STRUCTURE OF DESIGN MODELS*

SYSTEM DEFINITIONS	POLES	ZEROS
SISO SYSTEM A		
OPERATING-	526	-7.37
CONDITION:	-3.64	$-.86 \pm j6.84$
90% N_g	$-5.07 \pm j15.8$	$-.18 \pm j34.2$
CONTROL: W_f	$-.62 \pm j404$	
OUTPUT: N_p		
MIMO SYSTEM B		
OPERATING	-.482	
CONDITION:	-1.92	$-.84 \pm j6.85$
83% N_g	-10.0	
CONTROLS: W_f, V_g	$-5.07 \pm j15.8$	$-.18 \pm j34.2$
OUTPUTS: N_p, $T_{4.5}$	$-.62 \pm j40.4$	
MIMO SYSTEM C		
OPERATING-	.526	.199
CONDITION:	-2.2	$-.85 \pm j6.85$
90% N_g	-10.0	
CONTROLS: W_f, V_g	$-5.07 \pm j15.8$	$-.18 \pm j34.2$
OUTPUTS: N_p, $T_{4.5}$	$-.62 \pm j40.4$	

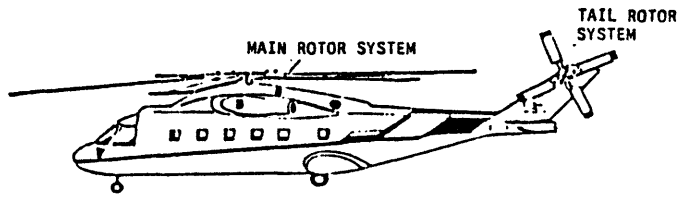

Figure 1. Conventional Single Main Rotor Helicopter

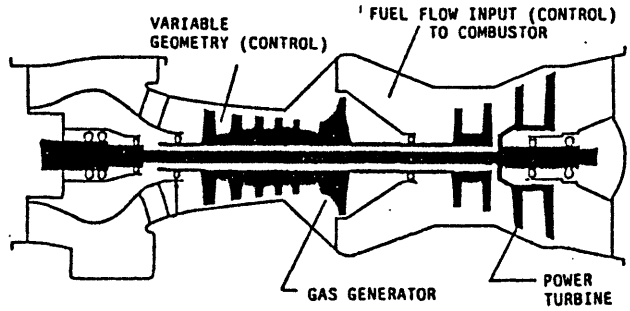

Figure 2. GE T700 Simplified Cross Section

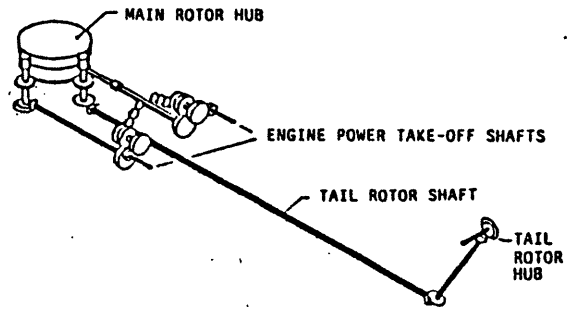

Figure 3. Helicopter Rotor System Drive-Train Isometric Diagram

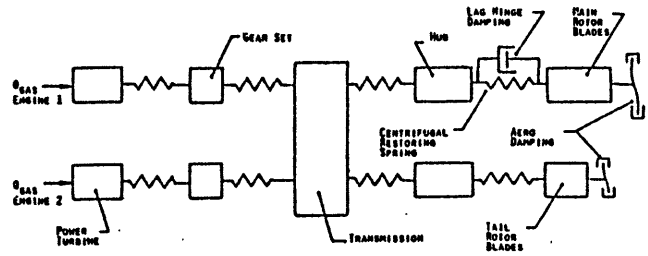

Figure 4. Lumped Parameter Representation of Helicopter Rotor System Drive Train

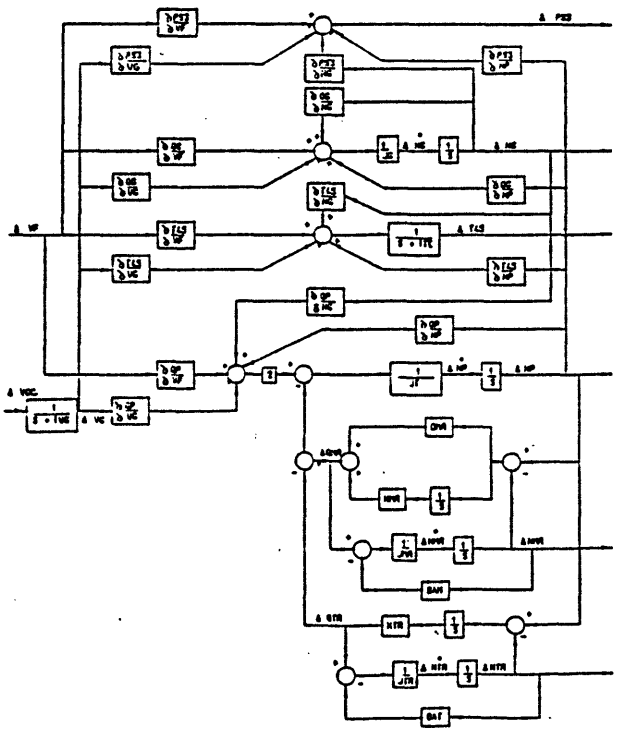

Figure 5. Block Diagram Representation of Coupled Turboshaft Engine Rotor System

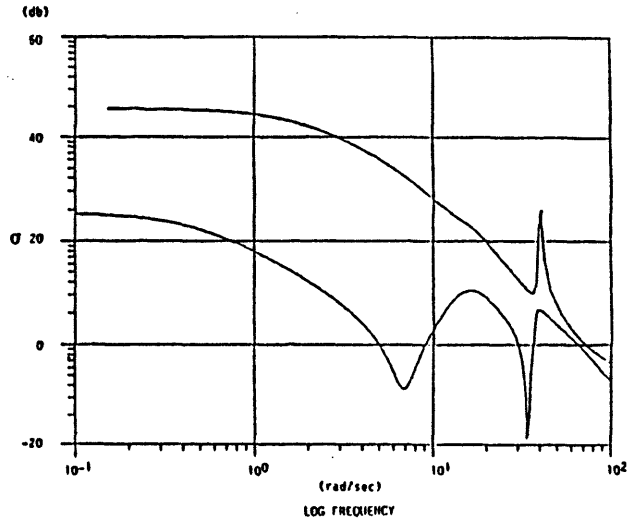

Figure 7. Singular Value Plot of the Open-Loop Transfer Function for the MIMO System B

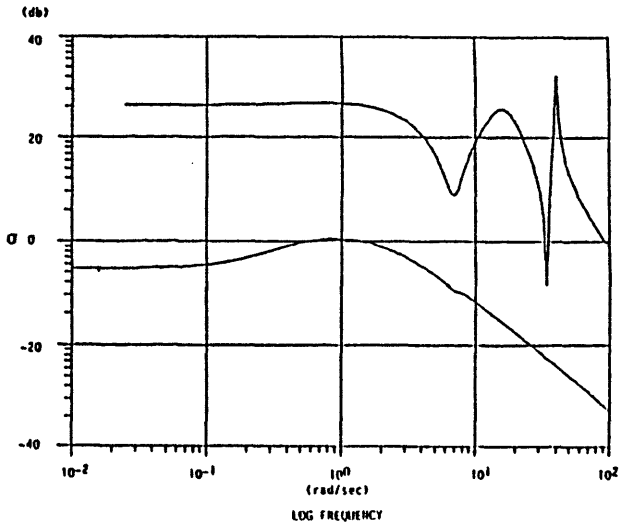

Figure 8. Singular Value Plot of the Open-Loop Transfer Function for the MIMO System C

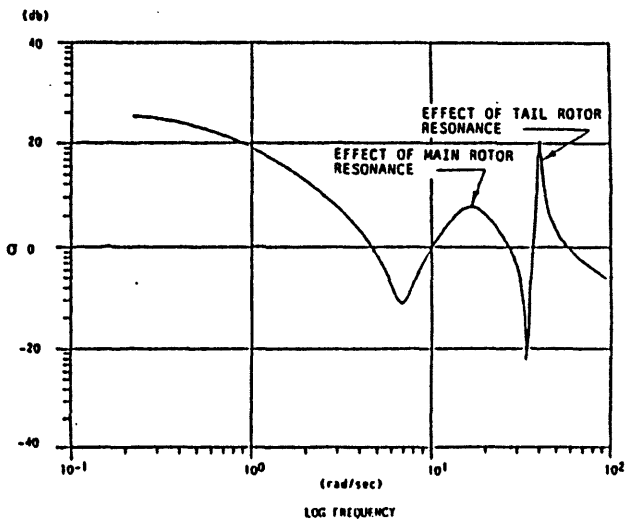

Figure 6. Magnitude Bode Plot of the Open-Loop Transfer Function for the SISO System A

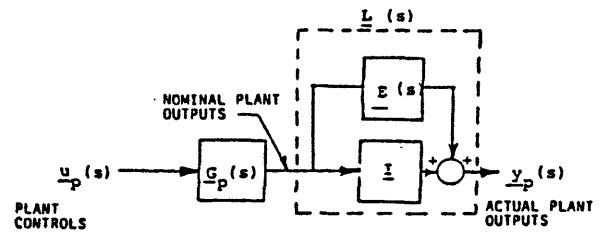

Figure 9. Modeling Error Definition

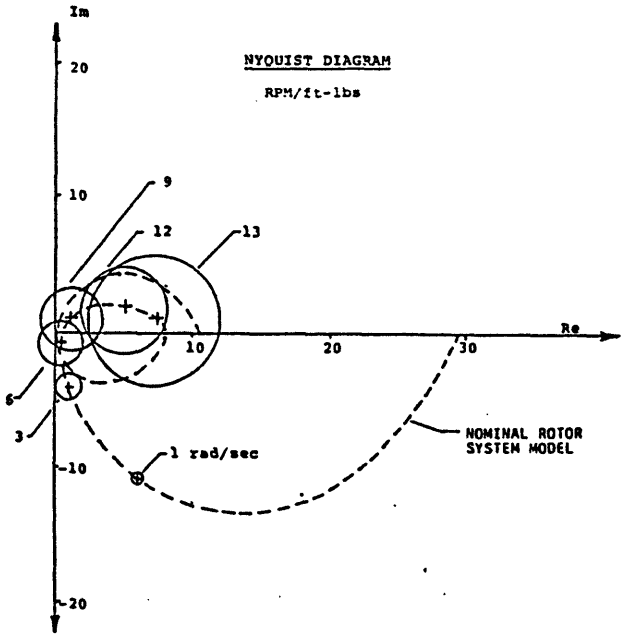

Figure 10. Depiction of Rotor System Unstructured Modeling Error

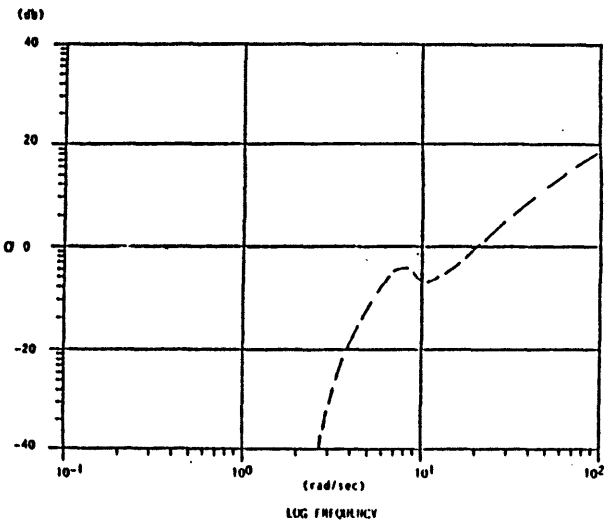

Figure 11. Bound on Multiplicative Error Versus Frequency

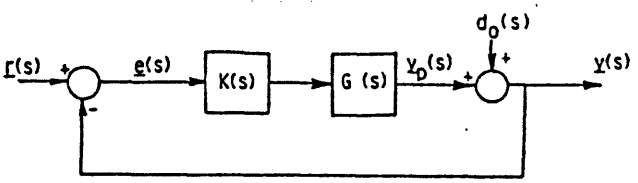

Figure 12. Feedback System Definition

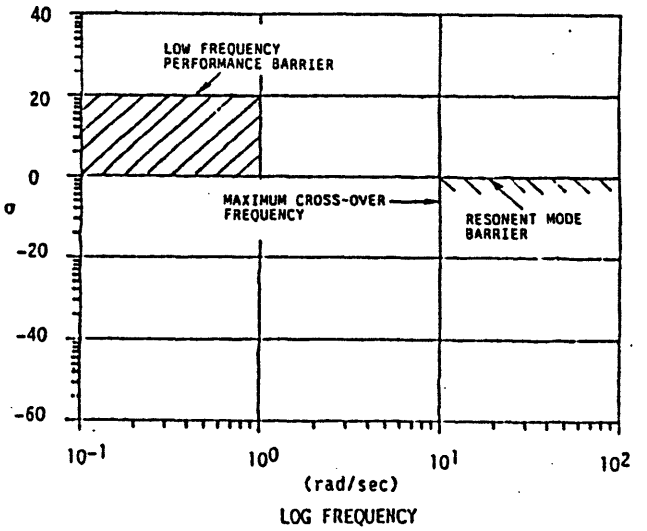

Figure 13. Frequency Domain Design Specifications

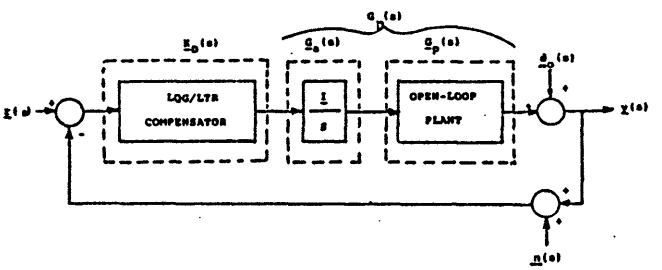

Figure 14. Control Structure Utilized in Design Process

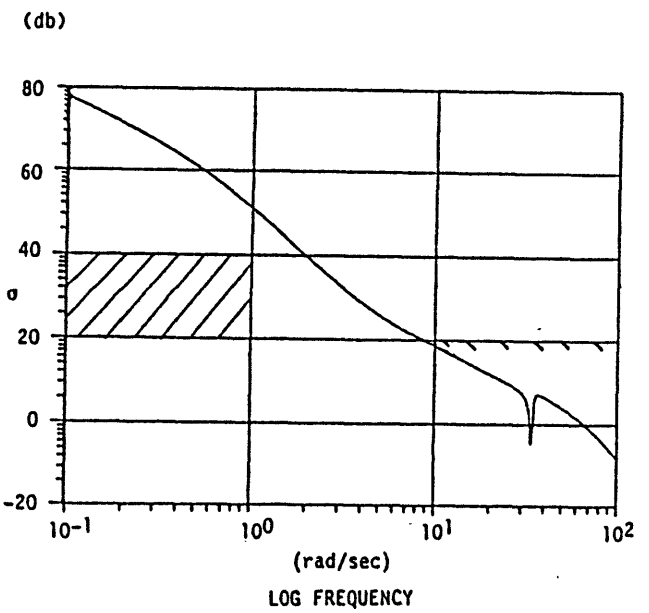

Figure 15. Magnitude of SISO Loop Transfer Function $g(j\omega)\,k(j\omega)$ from LQG/LTR Design A

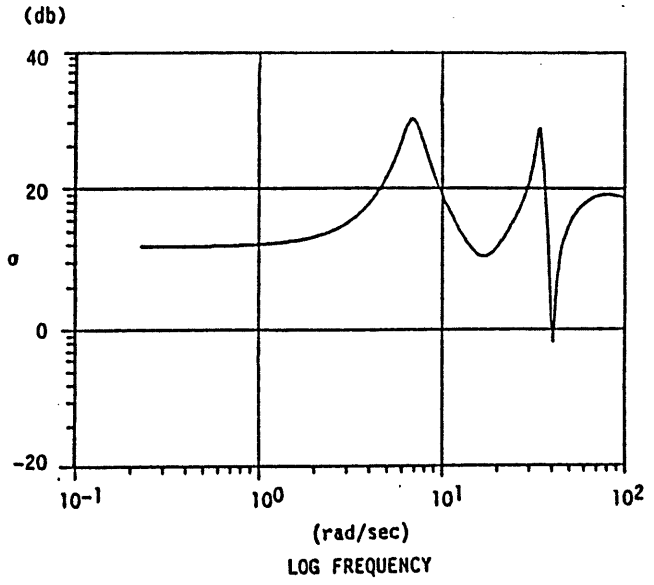

Figure 16. SISO LQG/LTR Compensator $k_D(j\omega)$ Magnitude vs. Frequency for Design A

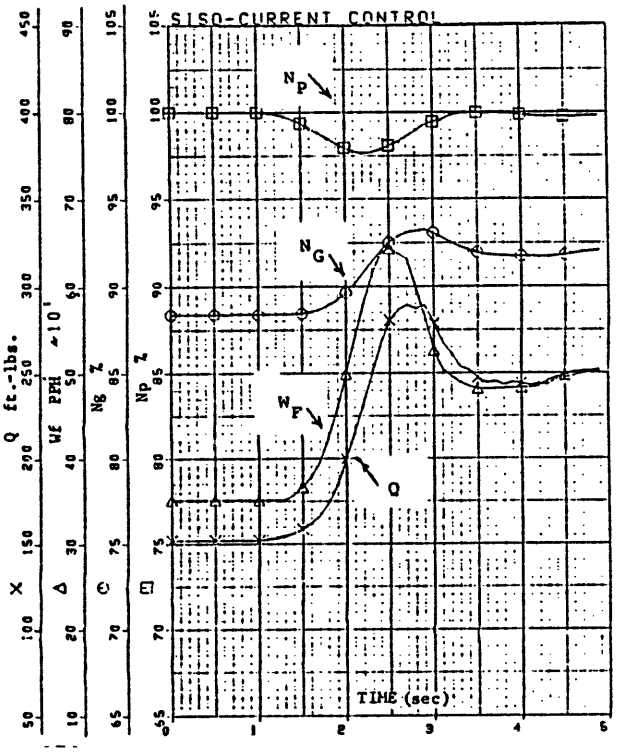

Figure 18a. Non-linear Simulation of Current Controller Compensated System Response to 30% Load Demand in 1 Second

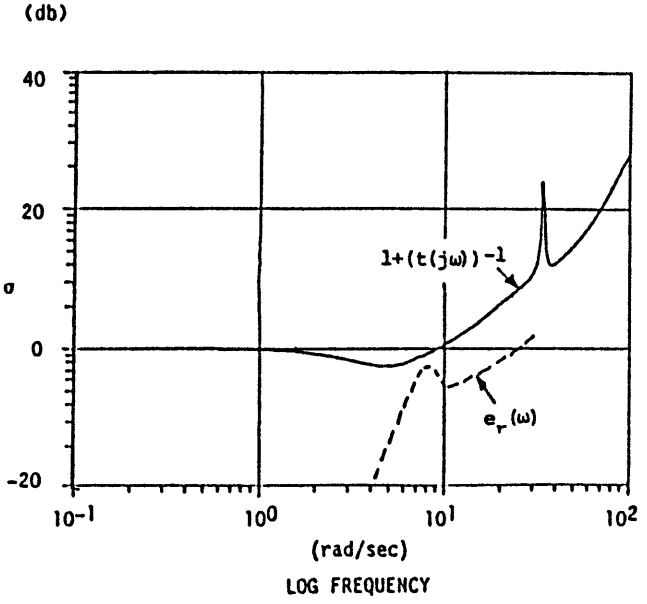

Figure 17. Stability Robustness Check for Design A

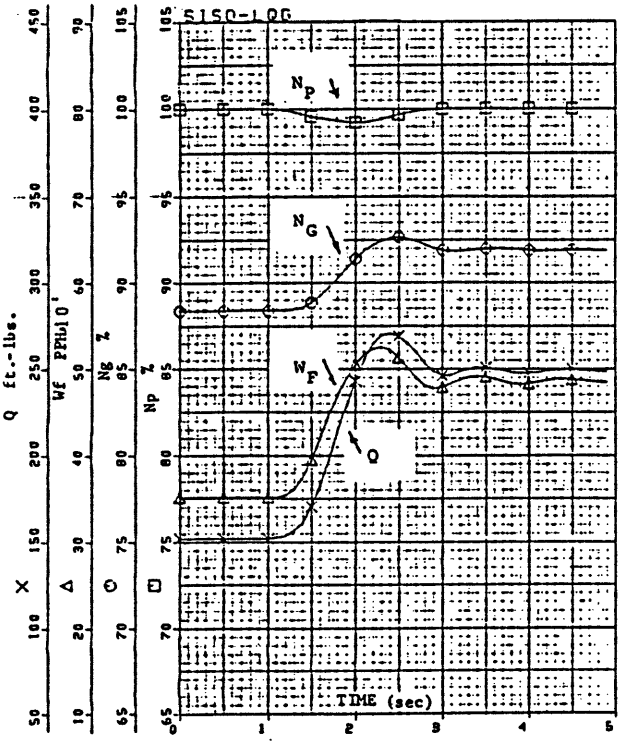

Figure 18b. Non-linear Simulation of SISO LQG/LTR Compensated System A Response to 30% Load Demand in 1 Second

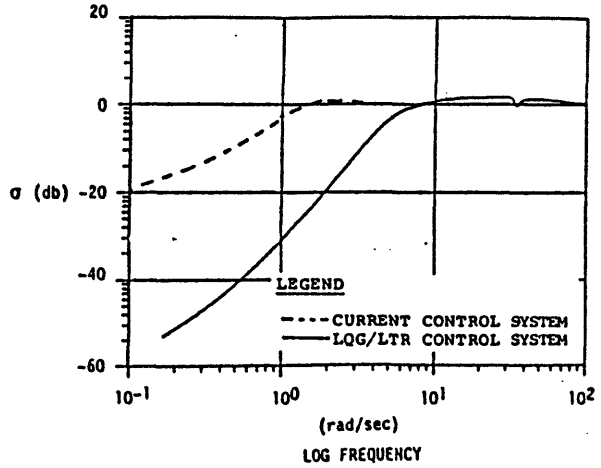

Figure 18c. Comparison of the Sensitivity Transfer Functions of the Current and LQT/LTR Control System Design A

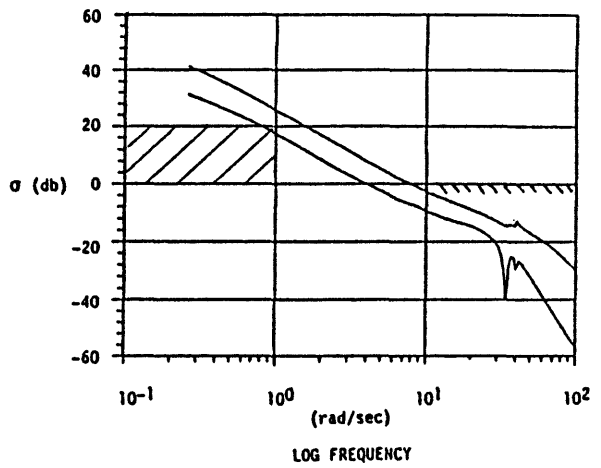

Figure 19. Singular Values of Loop Transfer Function $\underline{G}(j\omega)\,\underline{K}(j\omega)$ for Design B Using LQG/LTR Compensator

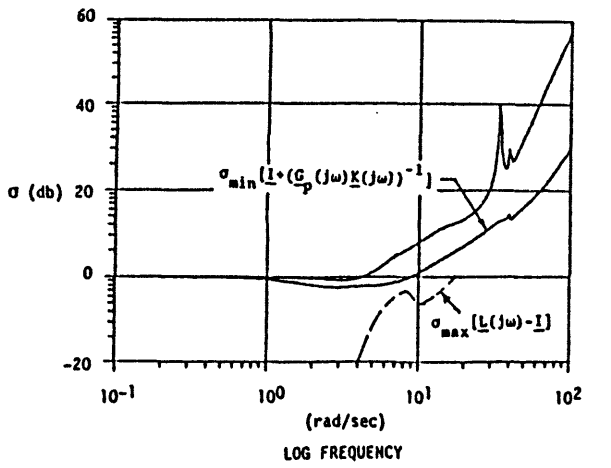

Figure 20. Stability Robustness Check for Design B

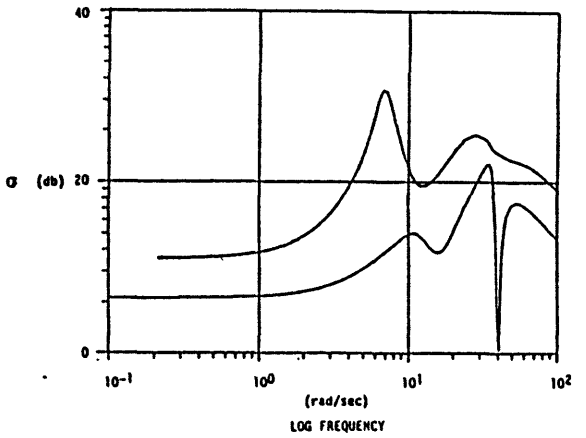

Figure 21. Singular Values of LQT/LTR Compensator $\underline{K}_D(j\omega)$ for Design B

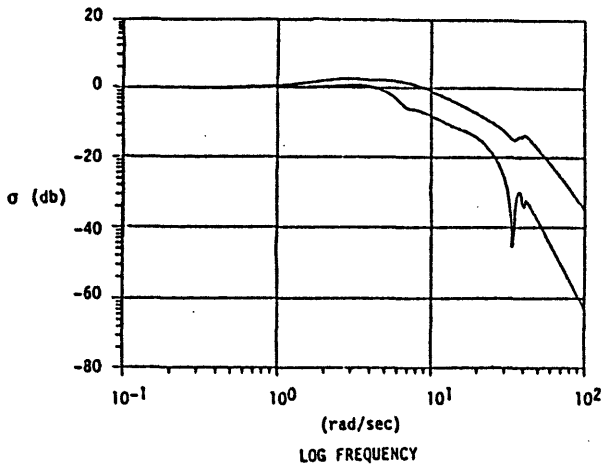

Figure 22. Singular Values of Closed-Loop Transfer Function $\underline{G}(j\omega)\,\underline{K}(j\omega)\,[\underline{I}+\underline{G}(j\omega)\,\underline{K}(j\omega)]^{-1}$ of Design B

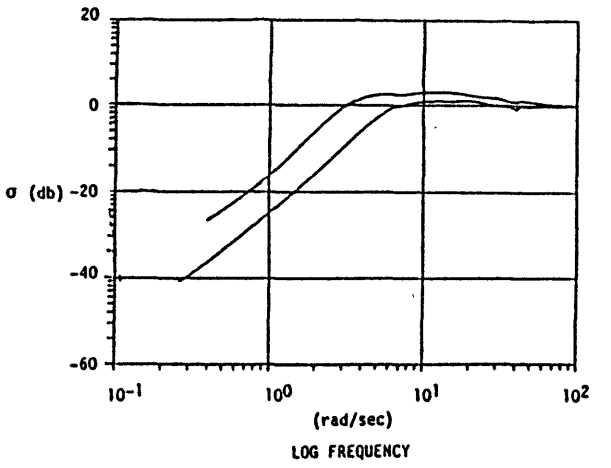

Figure 23. Singular Values of the Sensitivity Transfer Function $[\underline{I}+\underline{G}(j\omega)\,\underline{K}(j\omega)]^{-1}$ of Design B

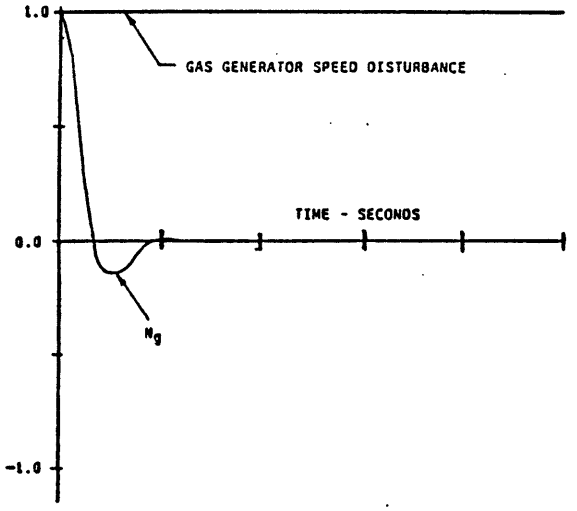

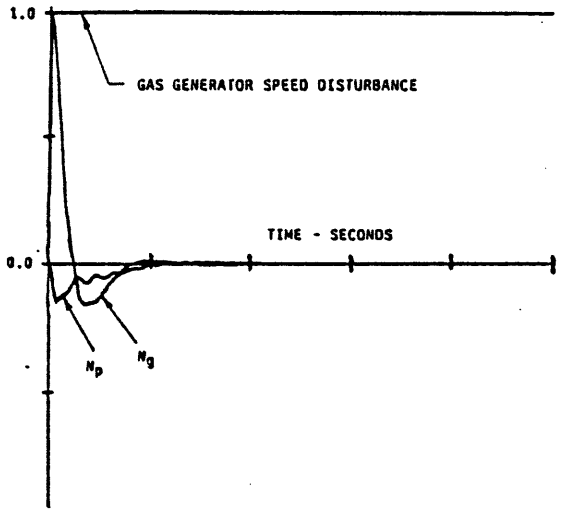

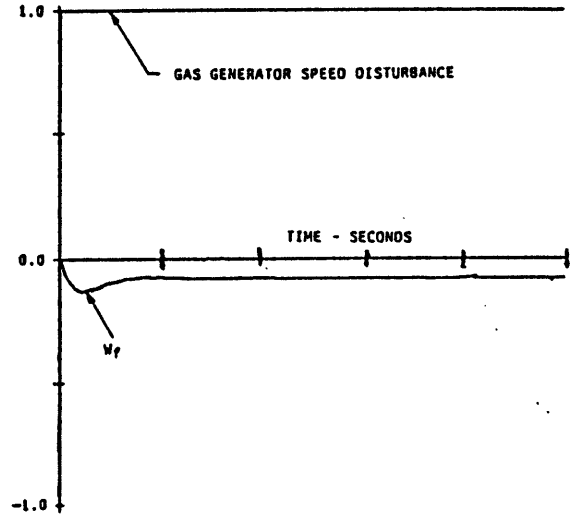

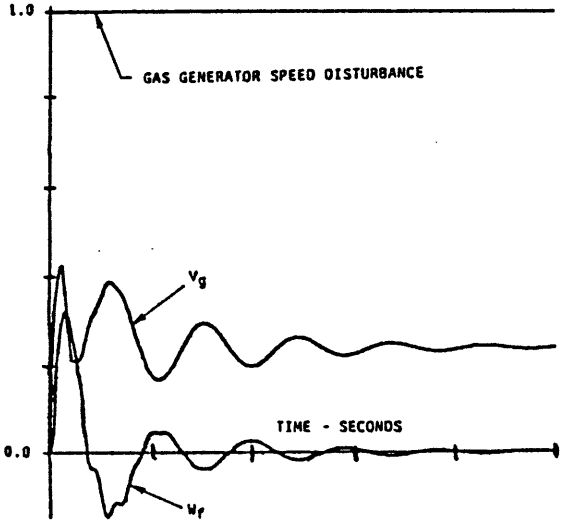

Figure 24a. Linear Simulation of a Step Response of SISO System A Response to a Gas Generator Speed Disturbance

Figure 24b. Linear Simulation of a Step Response of MIMO System B Response to a Gas Generator Speed Disturbance

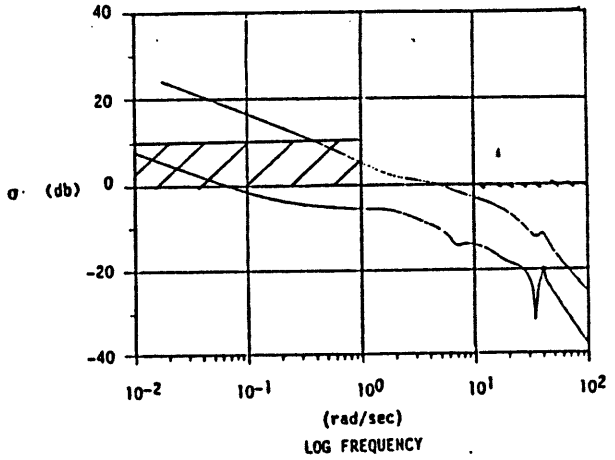

Figure 25. Singular Values of Loop Transfer Function $\underline{G}(j\omega)\,\underline{K}(j\omega)$ for Design C Using LQG/LTR Compensator

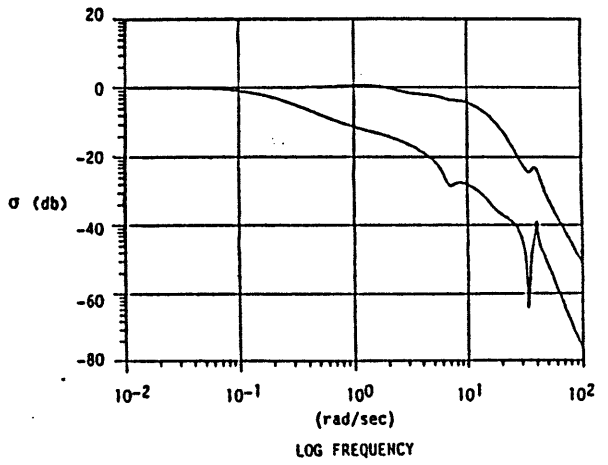

Figure 27. Singular Values of Closed-Loop Transfer Function $\underline{G}(j\omega)\,\underline{K}(j\omega)\,[\underline{I} + \underline{G}(j\omega)\,\underline{K}(j\omega)]^{-1}$ of Design C

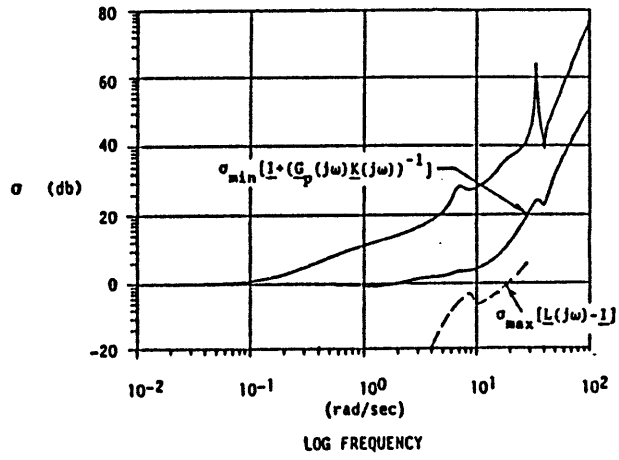

Figure 26. Stability Robustness Check for Design C

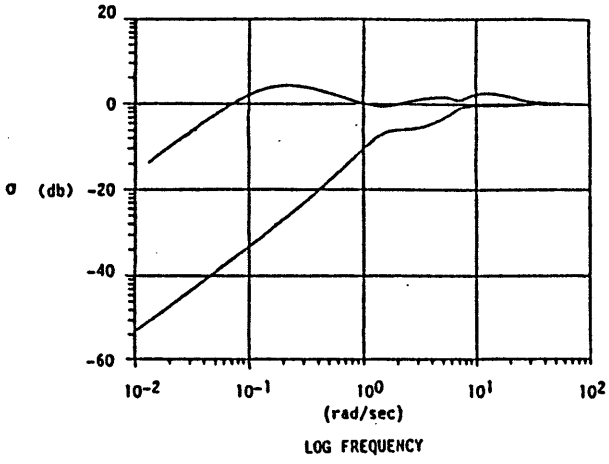

Figure 28. Singular Values of the Sensitivity Transfer Function $[\underline{I} + \underline{G}(j\omega)\,\underline{K}(j\omega)]^{-1}$ of Design C

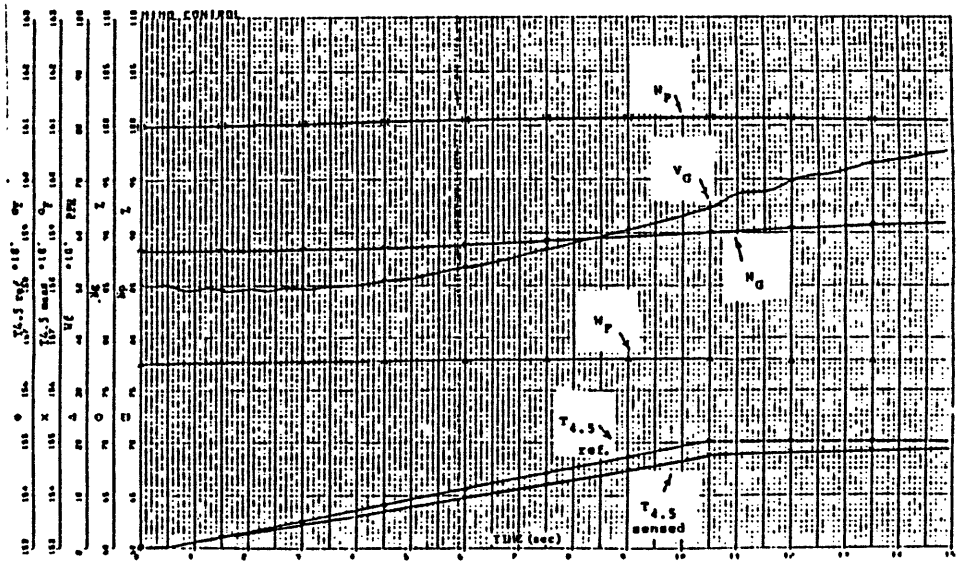

Figure 29. Non-Linear Simulation of Response of MIMO System C to a Slow Temperature Reference Ramp

APPENDIX A

STATE EQUATION

$$\frac{d}{dt}\begin{bmatrix} N_g \\ N_p \\ Q_{MR} \\ N_{MR} \\ Q_{TR} \\ N_{TR} \\ V_g \\ T_{4.5} \end{bmatrix} = \begin{bmatrix} \frac{1}{J_g}\frac{\partial Q_g}{\partial N_g} & 0 & 0 & 0 & 0 & 0 & \frac{1}{J_g}\frac{\partial Q_g}{\partial V_g} & 0 \\ \frac{2}{J_T}\frac{\partial Q_p}{\partial N_g} & \frac{2}{J_T}\frac{\partial Q_p}{\partial N_p} & -\frac{1}{J_T} & 0 & 0 & 0 & \frac{2}{J_T}\frac{\partial Q_p}{\partial V_g} & 0 \\ \frac{2D_{MR}}{J_T}\frac{\partial Q_p}{\partial N_g} & K_{MR} + \frac{2D_{MR}}{J_T}\frac{\partial Q_p}{\partial N_p} & \frac{-D_{MR}}{J_T} & -K_{MR} + \frac{D_{AM}D_{MR}}{J_{MR}} & 0 & 0 & \frac{2D_{MR}}{J_T}\frac{\partial Q_p}{\partial V_g} & 0 \\ 0 & 0 & \frac{1}{J_{MR}} & -\frac{D_{AM}}{J_{MR}} & 0 & 0 & 0 & 0 \\ 0 & K_{TR} & 0 & 0 & 0 & -K_{TR} & 0 & 0 \\ 0 & 0 & 0 & 0 & \frac{1}{J_{TR}} & -\frac{D_{AT}}{J_{TR}} & 0 & 0 \\ 0 & 0 & 0 & 0 & 0 & 0 & -T_{VG} & 0 \\ \frac{\partial T_{4.5}}{\partial N_g} & 0 & 0 & 0 & 0 & 0 & \frac{\partial T_{4.5}}{\partial V_g} & -T_{TC} \end{bmatrix} \begin{bmatrix} N_g \\ N_p \\ Q_{MR} \\ N_{MR} \\ Q_{TR} \\ N_{TR} \\ V_g \\ T_{4.5} \end{bmatrix} + \begin{bmatrix} \frac{1}{J_g}\frac{\partial Q_p}{\partial W_f} & 0 \\ \frac{2}{J_T}\frac{\partial Q_p}{\partial W_f} & 0 \\ \frac{2D_{MR}}{J_T}\frac{\partial Q_p}{\partial W_f} & 0 \\ 0 & 0 \\ 0 & 0 \\ 0 & 0 \\ 0 & 1 \\ \frac{\partial T_{4.5}}{\partial W_f} & 0 \end{bmatrix} \begin{bmatrix} W_f \\ V_{gc} \end{bmatrix}$$

APPENDIX B

SISO SYSTEM A: $\underline{x}^T = [N_g\ N_p\ Q_{MR}\ N_{MR}\ Q_{TR}\ N_{TR}]$

A MATRIX

-3.64	0.00	0.00	0.00	0.00	0.00
3.51	-1.09	-60.00	0.00	-60.00	0.00
0.50	5.18	10.00	-5.20	0.00	0.00
0.00	0.00	9.06	-0.45	0.00	0.00
0.00	6.29	0.00	0.00	0.00	-6.29
0.00	0.00	0.00	0.00	186.00	-.371

B MATRIX

45.20
42.70
6.14
0.00
0.00
0.00

C MATRIX

0.00	1.00	0.00	0.00	0.00	0.00

MIMO SYSTEM B: (SCALED) $x^T = [N_g\ N_p\ Q_{MR}\ N_{MR}\ Q_{TR}\ N_{TR}\ V_g]$

A MATRIX

-1.92	0.00	0.00	0.00	0.00	0.00	8.09
3.24	-.727	-.1212	0.00	-.012	0.00	-13.5
234.00	2600	-10.0	-2600	0.00	0.00	-9.75
0.00	0.00	.018	-.450	0.00	0.00	0.00
0.00	31450	0.00	0.00	0.00	-31450	0.00
0.00	0.00	0.00	0.00	-.037	-.371	0.00
0.00	0.00	0.00	0.00	0.00	0.00	-10.0

B MATRIX

11.47	0.00
17.55	0.00
1267	0.00
0.00	0.00
0.00	0.00
0.00	0.00
0.00	10.0

C MATRIX

0.00	1.00	0.00	0.00	0.00	0.00	0.00
1.00	0.00	0.00	0.00	0.00	0.00	0.00

MIMO SYSTEM C: (SCALED) $\underline{x}^T = [N_g\ N_p\ Q_{MR}\ N_{MR}\ Q_{TR}\ N_{TR}\ T_{4.5}\ V_g]$

A MATRIX

-3.64	0.00	0.00	0.00	0.00	0.00	0.00	16.39
7.84	-1.09	-1.212	0.00	-.150	0.00	0.00	-34.3
56.7	259.	-10.0	-260.	0.00	0.00	0.00	-24.8
0.00	0.00	.1812	-.450	0.00	0.00	0.00	0.00
0.00	2516.	0.00	0.00	0.00	-2516	0.00	0.00
0.00	0.00	0.00	0.00	.465	-.371	0.00	0.00
-5.90	0.00	0.00	0.00	0.00	0.00	-2.20	24.7
0.00	0.00	0.00	0.00	0.00	0.00	0.00	-10.0

B MATRIX

1.01	0.00
2.14	0.00
5.35	0.00
0.00	0.00
0.00	0.00
0.00	0.00
3.74	0.00
0.00	10.0

C MATRIX

0.00	1.00	0.00	0.00	0.00	0.00	0.00	0.00
0.00	0.00	0.00	0.00	0.00	0.00	1.00	0.00